

Dipole effects on molecular and electronic structures in a novel conjugate of oligo(phenyleneethynylene) and helical peptide

Hidenori Nakayama, Tomoyuki Morita and Shunsaku Kimura*

Received 8th October 2008, Accepted 12th February 2009

First published as an Advance Article on the web 10th March 2009

DOI: 10.1039/b817685j

A novel conjugate of a helical nonapeptide and an oligo(phenyleneethynylene) (OPE) having a nitro group at a molecular terminal was synthesized. Both components have a dipole. The peptide has a disulfide group at the N-terminal for immobilization on gold. In order to investigate the electric field effect of the helical peptide dipole on the OPE and molecular structure by the dipole–dipole interaction between the two components, the electronic structure of the OPE was spectroscopically studied in solution, the self-assembled monolayer on gold, and Langmuir–Blodgett (LB) layers on a fused quartz surface. The absorption maximum (λ_{max}) of the OPE component in chloroform is red-shifted by 4 nm from the reference OPE derivative without the helical peptide component. The red shifts of the OPE component are also observed in the LB monolayer and bilayer compared with that of the self-assembled monolayer. The observed dipole effect of the peptide on the OPE electronic structure was quantitatively discussed with *ab initio* calculations. Antiparallel orientation on the dipole directions of the peptide and the OPE components is considered to explain the red shifts *via* the dipole effect on the electronic structure of the OPE.

Introduction

Well-defined structures in nanometer sizes have been of great interest for developments of functional materials and devices in various fields from medical applications¹ to electronics.² Organic molecules have several advantages for construction of those structures, because they are nearly free to design their size, shape, and properties, and above all, self-assembling mechanisms can be integrated in them to build up a regular structure in a long range. Electronics is one of the areas where urgent developments of nanometer-scaled materials are highly required. As predicted by Moore, the number of processors in a unit area have been exponentially increasing for more than 30 years.³ However, the conventional top–down strategy for making semiconductor devices in more precise patterns and structures will face unavoidable problems in the near future.⁴ To overcome these problems, molecular electronics, which handles a single or a few organic molecules for electronic elements, is expected to provide novel molecular devices. Various organic molecules have been studied as candidates for them, π -conjugate oligomers, DNAs,⁵ and peptides⁶ for electronic wires, donor–acceptor conjugates for diodes,⁷ and rotaxanes⁸ and catenanes⁹ for switches and memories. Especially, the π -conjugate oligomers, oligo(phenylenevinylene)s¹⁰ and oligo(phenyleneethynylene)s¹¹ (OPEs), have been most intensively studied so far to show high conductivities and small distance dependency for the electron transfer reaction, which are properties required for molecular wires.

Molecular electronics has another challenge to integrate molecules into a functionally organized system. For this purpose, the molecules should have well-specified structures to be arranged regularly in space with help of noncovalent interactions, as demonstrated in sophisticated systems in nature. Helical peptides are a good example of building up the frame of protein structures in angstrom precision with taking a cylindrical shape. Inspired by such a nature's strategy, hydrogen-bonds¹², electrostatic interactions¹³, and CH– π interactions¹⁴ have been used for regulation of the artificial molecular structures. Recently, we have successfully utilized another noncovalent interaction, dipole–dipole interaction, for construction of a planar triangle geometry where three helices were circularly arranged in a head-to-tail manner.^{15,16}

We report here another example of a conformational regulation by dipole–dipole interaction between two different types of dipolar components in a single molecule. A novel conjugate of a helical nonapeptide and a nitro-substituted OPE is synthesized (**OPEn9**, Fig. 1). Both components have different magnitudes of dipoles. The peptide consists of an alternating sequence of alanine (Ala) and α -aminoisobutyric acid (Aib) with interruption of a glutamine at the center of the sequence. The OPE component is connected to the peptide *via* the glutamine. A disulfide group is attached to the N terminal of the peptide component for immobilization to gold in the case of formation of a self-assembled monolayer (SAM). The helical peptide and the OPE with the nitro substitution have dipoles of *ca.* 20 D and *ca.* 3.5 D, respectively. It is expected that the peptide and the OPE components may take antiparallel arrangement by the dipole–dipole interaction (Fig. 1) to form a planar structure which is suitable for self-assembling *via* stacking one over the other. A reference compound without the peptide moiety is also prepared (**OPEnAc**, Fig. 1).

Graduate School of Engineering, Kyoto University,
Kyoto-Daigaku-Katsura, Nishikyo-ku, 615-8510, Kyoto, Japan.
E-mail: shun@scl.kyoto-u.ac.jp

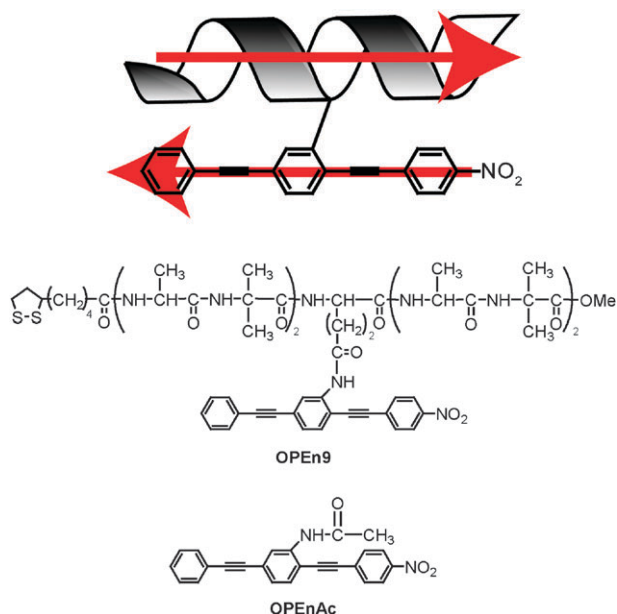


Fig. 1 Schematic illustration of a dipole–dipole interaction in **OPEn9** (top) and chemical structures of **OPEn9** (middle) and **OPEnAc** (bottom).

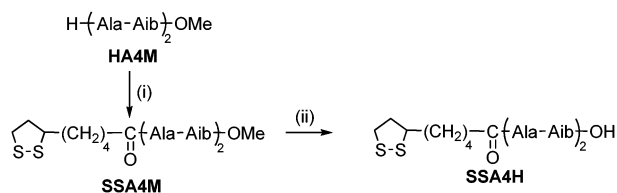
We study the electronic structure of the OPE in the conjugate in various environments of solution, Langmuir–Blodgett (LB) layers on fused quartz, and a SAM on gold. We discuss the dipole effects of the peptide in those environments to demonstrate the utility of dipole–dipole interaction for regulating the molecular structure.

Experimental

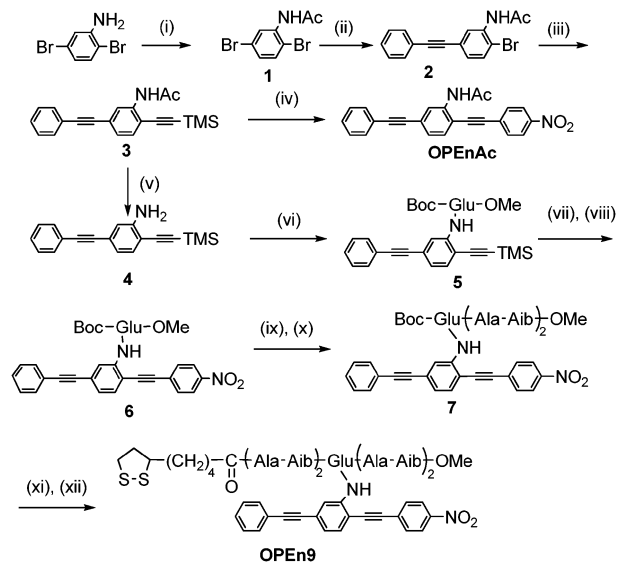
Materials

OPEn9 and **OPEnAc** were synthesized according to Schemes 1 and 2. The peptide component of **OPEn9** was synthesized by the conventional liquid-phase method. The OPE component of **OPEn9** and **OPEnAc** was synthesized by the Sonogashira coupling. Tetrahydrofuran (THF) used as solvent in the Sonogashira coupling was distilled from calcium hydride and butylated hydroxyl toluene. The other reagents were used as purchased. All intermediates were identified by ^1H NMR spectroscopy (Bruker DPX-400) and some of them were further confirmed by fast atom bombardment (FAB) mass spectrometry (JEOL JMS-HX110A). The purity of the products was checked by thin layer chromatography (TLC).

SSA4M. To a 50 mL two-neck round-bottom flask were added hydrochloric acid salt of HA4M¹⁵ (130 mg, 0.33 mmol),



Scheme 1 Reagents and conditions: (i) DL-lipoic acid, *O*-(7-azabenzotriazol-1-yl)-1,1,3,3-tetramethyluronium hexafluorophosphate (HATU), diisopropylethylamine (DIEA), DMF, rt, 80%. (ii) 1 N NaOH aqueous solution, methanol, dioxane.



Scheme 2 Reagents and conditions: (i) acetic anhydride, water, reflux, 3 h, 92%, (ii) phenylacetylene, bis(triphenylphosphine) palladium(ii) dichloride ($\text{Pd}(\text{PPh}_3)_2\text{Cl}_2$), copper(i) iodide (CuI), DIEA, THF, 75 °C, 3 d, (iii) trimethylsilylacetylene, $\text{Pd}(\text{PPh}_3)_2\text{Cl}_2$, CuI, DIEA, THF, 2.5 d, 12% in two steps, (iv) potassium carbonate (K_2CO_3), methanol, dichloromethane, 1 h, and then 4-iodonitrobenzene, $\text{Pd}(\text{PPh}_3)_2\text{Cl}_2$, CuI, DIEA, THF, rt, 3 h, 17%, (v) 1.8 M HCl aqueous solution, THF, reflux, 12 h, (vi) Boc-Glu-OMe, HATU, DIEA, DMF, 60 °C, 1.5 d, 61%, (vii) K_2CO_3 , methanol, dichloromethane, rt, 3 h, 68%, (viii) 4-iodonitrobenzene, $\text{Pd}(\text{PPh}_3)_2\text{Cl}_2$, CuI, DIEA, THF, 40 °C, 20 h, 78%, (ix) 1 N NaOH aqueous solution, methanol, dioxane 11 h, (x) HA4M, HATU, DIEA, DMF, rt, 1 d, 58%, (xi) trifluoroacetic acid, anisole, 0 °C, 0.5 h, (xii) SSA4H, HATU, DIEA, DMF, rt, then 40 °C, 28 h, 40%.

D,L-lipoic acid (100 mg, 0.49 mmol), *O*-(7-azabenzotriazol-1-yl)-1,1,3,3-tetramethyluronium hexafluorophosphate (HATU, 250 mg, 0.66 mmol), *N,N*-diisopropylethylamine (DIEA, 200 μL , 1.15 mmol) at 0 °C. The reaction mixture was stirred under argon atmosphere for 14 h and concentrated under reduced pressure. The residue was taken up with chloroform and washed successively with 4% NaHCO_3 aq. (3 \times), the brine, 4% KHSO_4 aq. (2 \times), and the brine. The organic layer was dried over MgSO_4 and concentrated under reduced pressure. The crude product was purified by column chromatography (silica gel, eluent: chloroform/methanol = 50/1 and then 10/1). The product was obtained as transparent oil (140 mg, 80%). δ_{H} (400 MHz; CDCl_3 ; Me_4Si) 1.31–1.29 (6 H, m, $\text{Ala}^{\text{C}^\beta}$), 1.45–1.43(12 H, m, $\text{Aib}^{\text{C}^\beta}$), 1.61 (4 H, m, $\text{SSCH}_2\text{CH}_2\text{CH}(\text{CH}_2)_3\text{CH}_2\text{CO}$), 1.85 (1 H, m, $\text{SSCH}_2\text{CH}_2\text{CH}(\text{CH}_2)_3\text{CH}_2\text{CO}$), 2.39 (1 H, m, $\text{SSCH}_2\text{CH}_2\text{CH}(\text{CH}_2)_3\text{CH}_2\text{CO}$), 3.06 (2 H, m, $\text{SSCH}_2\text{CH}_2\text{CH}(\text{CH}_2)_3\text{CH}_2\text{CO}$), 3.49 (1 H, m, $\text{SSCH}_2\text{CH}_2\text{CH}(\text{CH}_2)_3\text{CH}_2\text{CO}$), 3.64 (3 H, s, OCH_3), 4.18 (1 H, m, $\text{Ala}^{\text{C}^\alpha}$), 4.33 (1 H, m, $\text{Ala}^{\text{C}^\alpha}$), 5.83 (1 H, d, Ala^{NH}), 6.54 (1 H, s, Aib^{NH}), 6.72 (1 H, d, Ala^{NH}), 6.95 (1 H, s, Aib^{NH}); m/z (FAB; 3-nitrobenzyl alcohol (NBA) as matrix) 533.4 ($(\text{M} + \text{H})^+$). $\text{C}_{23}\text{H}_{41}\text{N}_4\text{O}_6\text{S}_2$ requires 533.2).

SSA4H. To a 50 mL round-bottom flask were added SSA4M (120 mg, 225 μmol), 1 N NaOH aq. (450 μL),

methanol (900 μL), dioxane (900 μL). The reaction mixture was stirred for 6 h and neutralized with 1 N HCl aq., and then the solution was concentrated under reduced pressure. The residue was taken up with chloroform/methanol and the residual salt was filtered out, and the filtrate was concentrated in reduced atmosphere. The obtained crude product was used in the next step without further purification.

1. To a 500 mL round-bottom flask equipped with a water-cooled Dimroth condenser were added 2,5-dibromoaniline (10 g, 39.8 mmol), acetic anhydride (40 mL), and water (40 mL). The mixture was refluxed for 4.5 h and poured into 400 mL of water. The precipitation was collected with a filter and dried in vacuum. The product was obtained as a white solid (10.8 g, 92%). δ_{H} (400 MHz; CDCl_3 ; Me_4Si) 2.24 (3 H, s, COCH_3), 7.11 (1 H, dd, benzene), 7.39 (1 H, d, benzene), 7.56 (1 H, br s, benzene), 8.59 (1 H, br s, ArNHCOCH_3).

2. To a flame-dried three-neck round-bottom flask equipped with a water-cooled Dimroth condenser and a dropping funnel were added **1** (10.14 g, 37.2 mmol), copper(I) iodide (CuI) (0.66 g, 3.46 mmol), bis(triphenylphosphine)palladium(II) chloride ($\text{Pd}(\text{PPh}_3)_2\text{Cl}_2$, 1.46 g, 2.08 mmol), DIEA (24.1 mL, 138 mmol), and THF (150 mL). The solution was stirred at 75 $^\circ\text{C}$ under argon atmosphere. Phenylacetylene (4.08 mL, 37.2 mmol) which was dissolved in 40 mL of THF was added to the solution over 15 h, and the solution was stirred for 45 h. Then the reaction mixture was filtered and dried under reduced pressure. The residue was purified by flash column chromatography (silica gel, eluent: ethyl acetate/hexane = 1/3 v/v) twice. The obtained mixture of the product and byproduct, 2,5-di(ethynylphenyl)acetanilide, (5.32 g) was used in the next reaction without additional purification.

3. To a flame-dried two-neck round-bottom flask equipped with a water-cooled Dimroth condenser were added the mixture of **2** and 2,5-di(ethynylphenyl)acetanilide obtained above (5.32 g), trimethylsilylacetylene (5.1 mL, 36 mmol), CuI (323 mg, 1.7 mmol), $\text{Ph}(\text{Ph}_3)_2\text{Cl}_2$ (713 mg, 1.0 mmol), DIEA (11.8 mL, 98 mmol), and THF (50 mL). The solution was stirred at 70 $^\circ\text{C}$ under argon atmosphere for 3 d. The precipitate was filtered off and the solvent of the filtrate was removed under reduced pressure. The residue was purified by column chromatography (silica gel, eluent: ethyl acetate/hexane = 1/3 v/v) to obtain the product (2.53 g, 22%). δ_{H} (400 MHz; CDCl_3 ; Me_4Si) 0.25 (9 H, s, $(\text{CH}_3)_3\text{SiCC}$), 2.24 (3 H, s, CH_3CONH), 7.16 (1 H, dd, benzene), 7.40 (4 H, m, benzene), 7.72 (2 H, m, benzene), 7.91 (1 H, br s, CH_3CONH), 8.53 (s, 1H, benzene); m/z (FAB; dithiothreitol/ α -thioglycerol = 1/2 (DTT/TG) as matrix) 332.19 ($(\text{M} + \text{H})^+$. $\text{C}_{21}\text{H}_{22}\text{NOSi}$ requires 332.14).

4. To a 500 mL round-bottom flask equipped with a water-cooled Dimroth condenser were added **3** (2.20 g, 6.64 mmol), THF (120 mL), 1.2 M HCl aq. (120 mL). The mixture was refluxed for 12 h and the solvent was removed under reduced pressure. The residue was purified by column chromatography (silica gel, eluents: dichloromethane/hexane = 1/1 v/v, and then dichloromethane). Due to some side reactions,^{11b} the product was not completely purified by column chromatography. The crude product was used in the next step without further purification.

5. To a 100 mL round-bottom flask were added **4** (500 mg, 1.73 mmol), Boc-Glu-OMe (1.13 g, 4.32 mmol), HATU (2.46 g, 6.49 mmol), and DMF (40 mL). DIEA (1.69 mL, 9.73 mmol) was added to the reaction solution dropwise at room temperature under argon atmosphere and then the mixture was kept at 60 $^\circ\text{C}$ for 12 h. The solution was concentrated in reduced atmosphere. The residue was taken up with chloroform, and then the precipitate was filtered off. The filtrate was washed successively with water, 4% NaHCO_3 aq. (3 \times), the brine, 4% KHSO_4 aq., and the brine. The organic layer was dried over MgSO_4 and concentrated under reduced pressure. The residue was purified by column chromatography (silica gel, eluant: ethyl acetate/hexane = 1/3 v/v). The product was obtained as colorless oil (560 mg, 61%). δ_{H} (400 MHz; CDCl_3 ; Me_4Si) 0.244 (9 H, s, $\text{Si}(\text{CH}_3)_3$), 1.38 (9 H, s, $\text{C}(\text{CH}_3)_3$), 2.49–2.04 (2 H, m, GluC^γ), 2.57 (2 H, m, GluC^β), 3.73 (1 H, s, OCH_3), 4.40 (1 H, s, GluC^α), 5.21 (1 H, s, urethane-NH), 7.17 (2 H, dd, benzene), 7.39–7.42 (4 H, m, benzene), 7.51–7.54 (2 H, m, benzene), 8.01 (1H, s, amide-NH), 8.52 (1 H, s, benzene); m/z (FAB; NBA as matrix) 532.3 (M^+ . $\text{C}_{30}\text{H}_{36}\text{N}_2\text{O}_5\text{Si}$ requires 532.24).

6. For deprotection of the trimethylsilyl group of **5**, to a 100 mL round-bottom flask were added **5** (560 mg, 1.05 mmol), potassium carbonate (435 mg, 3.15 mmol), methanol (20 mL), and dichloromethane (20 mL). The solution was stirred under argon atmosphere for 0.5 h, and poured into water and then extracted by ethyl acetate. The organic layer was washed with brine (3 \times). The brine solution was washed with ethyl acetate (3 \times). The combined organic layer was dried over MgSO_4 and concentrated under reduced pressure. The residue was purified by flash column chromatography (silica gel, eluent: ethyl acetate/hexane = 1/4 v/v). The product was obtained as a white solid (300 mg, 62%). Subsequently, to a 20 mL oven-dried round-bottom flask were added the deprotected product (300 mg, 0.65 mmol), 4-iodonitrobenzene (650 mg, 260 μmol), $\text{Pd}(\text{II})(\text{PPh}_3)_2\text{Cl}_2$ (27 mg, 40 μmol), CuI (12 mg, 65 μmol), DIEA (0.45 mL, 26 mmol), and THF (25 mL). The reaction solution was stirred under argon atmosphere at 40 $^\circ\text{C}$ for 20 h. The solution was then concentrated under reduced pressure and the residue was purified by column chromatography (silica gel, eluents: ethyl acetate/hexane = 1/2, 1/1, and then chloroform/methanol = 10/1 v/v). The product was obtained as a bright yellow solid (294 mg, 78%). δ_{H} (400 MHz; CDCl_3 ; Me_4Si) 1.39 (9 H, s, $\text{C}(\text{CH}_3)_3$), 2.05–2.54 (2 H, m, GluC^γ), 2.56–2.62 (2 H, m, GluC^β), 3.74 (1 H, s, OCH_3), 4.42 (1 H, s, GluC^α), 5.21 (1 H, s, urethane-NH), 7.27 (1 H, d, benzene), 7.40–7.42 (3 H, m, benzene), 7.50 (1 H, d, benzene), 7.55–7.57 (2 H, m, benzene), 7.97 (2 H, d, benzene), 8.10 (1 H, s, amide-NH), 8.23 (2 H, d, benzene), 8.66 (1 H, s, benzene); m/z (FAB; NBA as matrix) 582.1 (M^+ . $\text{C}_{33}\text{H}_{31}\text{N}_3\text{O}_7$ requires 582.11).

7. The methoxy group on **6** (100 mg, 17 mmol) was deprotected by treatment with 1 N NaOH aq. (0.35 mL) in a mixed solvent of dichloromethane, methanol, and 1,4-dioxane. After 4 h of stirring at room temperature, the solution was neutralized with 1 N HCl aq. and the solvent was removed under reduced pressure. The residue was washed with diethyl

ether. To a 30 mL round-bottom flask were added the product (100 mg, 170 μmol), hydrochloric acid salt of HA4M (100 mg), HATU (100 mg, 22.9 μmol), DIEA (100 μL , 61 μmol), and DMF (1 mL) at 0 $^{\circ}\text{C}$. The reaction solution was stirred under argon atmosphere for 1 d. The solution was concentrated under reduced pressure. The residue was taken up with chloroform and washed successively with 4% NaHCO_3 aq. (3 \times), brine, 4% KHSO_4 aq. (3 \times), and brine. The organic layer was dried over MgSO_4 and concentrated under reduced pressure. The obtained residue was purified by column chromatography (silica gel, eluants: chloroform/methanol = 75/1, 50/1, 40/1, and 30/1 v/v). The product was obtained as a yellow solid (86 mg, 58%). δ_{H} (400 MHz; CDCl_3 ; Me_4Si) 1.52–1.36 (27 H, m, AibC $^{\beta}$, Boc, AlaC $^{\beta}$), 2.18 (2 H, m, GluC $^{\beta}$), 2.72 (2 H, m, GluC $^{\gamma}$), 3.68 (3 H, s, OCH $_3$), 4.10–4.13 (2 H, m, AlaC $^{\alpha}$), 4.43 (1 H, t, GluC $^{\alpha}$), 6.37 (1 H, s, GluNH), 6.72 (1 H, d, AlaNH), 6.96 (1 H, d, AlaNH), 7.23 (1 H, m, benzene), 7.30–7.33 (3 H, m, benzene), 7.32–7.52 (3 H, m, benzene), 7.71 (2 H, d, benzene), 8.12 (1 H, s, benzene), 8.24 (2 H, d, benzene), 8.60 (1 H, s, ArNHCO(CH $_2$) $_2$); m/z (FAB; NBA) 894.4 ((M + H) $^{+}$). $\text{C}_{47}\text{H}_{56}\text{N}_7\text{O}_{11}$ requires 894.40).

OPEnAc. The trimethylsilyl group of **3** (100 mg, 0.30 mmol) was deprotected by treatment with potassium carbonate (83.4 mg, 0.60 mmol) in a mixed solvent of methanol (5 mL) and dichloromethane (5 mL) for 1 h. The reaction solution was then pored into water and extracted with ethyl acetate. The organic layer was washed with brine (3 \times) and dried over MgSO_4 . The solvent was removed under reduced pressure and the residue was dried in vacuum. The product was then mixed with *p*-iodonitrobenzene (150 mg, 0.60 mmol), Pd(PPh $_3$) $_2\text{Cl}_2$ (12.7 mg, 18 μmol), CuI (5.8 mg, 30 μmol), DIEA (0.21 mL, 1.2 mmol), and THF (5 mL) in a flame-dried 50 mL two-neck flask under argon atmosphere at 0 $^{\circ}\text{C}$. The solution was stirred at 0 $^{\circ}\text{C}$ for 1 h and then at room temperature for 2 h. The solution was then filtered and the filtrate was concentrated under reduced pressure. The residue was taken up with dichloromethane and washed with 4% KHSO_4 aq. (3 \times) and the brine. The organic layer was dried over MgSO_4 . The product was then purified with a silica gel column chromatography (eluent: dichloromethane) and Sephadex LH20 column (eluant: DMF). The product was obtained as a yellow solid (20 mg, 17%). δ_{H} (400 MHz; CDCl_3 ; Me_4Si) 2.28 (3 H, s, NHCOCH $_3$), 7.27 (1 H, s, benzene), 7.41 (3 H, m, benzene), 7.41–7.55 (4 H, m, benzene) 7.68 (2 H, d, benzene), 7.98 (1 H, br s, NHCOCH $_3$), 8.23 (1 H, d, benzene), 8.67 (1 H, br s, benzene); m/z (FAB; DTT/TG as matrix) 381.2 ((M + H) $^{+}$). $\text{C}_{24}\text{H}_{17}\text{N}_2\text{O}_3$ requires 381.12).

OPEn9. The Boc group on **7** (88 mg, 96 μmol) was deprotected by treatment with TFA/anisole for 0.5 h. The obtained product was washed with diethyl ether. The product was added to a test tube with SSA4H (95 mg, 185 μmol), HATU (105 mg, 277 μmol), DIEA (72 μL , 416 μmol), and DMF (*ca.* 10 mL) at 0 $^{\circ}\text{C}$, and the reaction solution was stirred for 27 h under argon atmosphere. The product was purified by a Sephadex LH20 column (eluent: DMF), silica gel column (eluants: chloroform/methanol = 75/1, 50/1, and 10/1 v/v), and Sephadex LH20 column (eluant: DMF). The product was

obtained as a yellow solid (25 mg, 40%). δ_{H} (400 MHz; CDCl_3 ; Me_4Si) 1.36–1.52 (45 H, m, AibC $^{\beta}$, Boc, AlaC $^{\beta}$), 1.67–1.69 (4 H, m, SSCH $_2\text{CH}_2\text{CH}(\text{CH}_2)_3\text{CH}_2\text{CO}$), 1.89–1.92 (1 H, m, SSCH $_2\text{CH}_2\text{CH}(\text{CH}_2)_3\text{CH}_2\text{CO}$), 2.35 (4 H, m, GluC $^{\beta}$ and SSCH $_2\text{CH}_2\text{CH}(\text{CH}_2)_3\text{CH}_2\text{CO}$), 2.45 (1 H, m, SSCH $_2\text{CH}_2\text{CH}(\text{CH}_2)_3\text{CH}_2\text{CO}$), 2.63–2.75 (2 H, m, GluC $^{\gamma}$), 3.11–3.16 (2 H, m, SSCH $_2\text{CH}_2\text{CH}(\text{CH}_2)_3\text{CH}_2\text{CO}$), 3.54 (1 H, m, SSCH $_2\text{CH}_2\text{CH}(\text{CH}_2)_3\text{CH}_2\text{CO}$), 3.60 (3 H, s, OCH $_3$), 3.88 (1 H, m, AlaC $^{\alpha}$), 3.99 (1 H, m, AlaC $^{\alpha}$), 4.15 (2 H, m, AlaC $^{\alpha}$ GluC $^{\alpha}$), 4.23 (1 H, m, AlaC $^{\alpha}$), 6.98–6.99 (2 H, m, AlaNH, AibNH), 7.14(1 H, d, AlaNH), 7.24 (1 H, m, benzene), 7.34–7.40 (2 H, m, benzene, AlaNH, AibNH), 7.43 (1 H, s, AibNH), 7.48 (2 H, d, benzene), 7.53–7.55 (2 H, m, benzene), 7.65–7.66 (3 H, m, benzene, GluNH), 7.73 (1 H, s, AibNH), 7.83 (1 H, d, AlaNH), 8.22 (2 H, d, benzene), 8.32 (1 H, s, benzene), 8.59 (1 H, s, ArNHCO(CH $_2$) $_2$); m/z (FAB; NBA) 1294.5 ((M + H) $^{+}$). $\text{C}_{64}\text{H}_{84}\text{N}_{11}\text{O}_{14}\text{S}_2$ requires 1294.5).

Spectroscopy in solution

The CD spectrum was measured by a JASCO J-600 CD spectropolarimeter at a residue concentration of 0.2 mM with an optical cell of a 0.1 cm optical path length. UV-vis absorption spectra were recorded on a Shimadzu UV-2450PC spectrometer at a concentration of less than 10 μM .

Quantum calculation

ab initio Calculations were carried out on a Gaussian, Inc. Gaussian 03¹⁷ program using the density functional theory (DFT) with Becke's three parameter hybrid functional and Lee–Yang–Parr correlation (B3LYP) method¹⁸ with the 6-31G(d,p)¹⁹ basis set. The calculations were performed on a Fujitsu HX600 cluster (operation system: RedHat Enterprise Linux AS V4). The geometry of **OPEnAc** was initially generated on a Semichem, Inc. Gaussview program (version 4.1.2)²⁰, and the geometry was optimized by the DFT method on Gaussian 03 and the frontier orbitals were visualized. The optimized geometry under no external electric field was checked by frequency analysis. It was confirmed there is no imaginary frequency number. The geometry was re-optimized under various external electric fields ($\sim 1 \times 10^9$ V m $^{-1}$) along the long axis to see its effect on the frontier orbital distributions. The direction of the electric fields (from positive to negative) is the same as the direction of the dipole moment of the OPE moiety (from negative to positive).

Preparation of LB layer

Langmuir layers of **OPEn9**, **OPEnAc**, and Boc-(Ala-Aib) $_4$ -OMe (**BA8M**) were prepared at the air/water interface, and the π -*A* isotherms were studied by a USI 3-22N Langmuir film balance with a trough of a 100 \times 278 mm area. Milli-Q water was used for the subphase. A chloroform solution of each compound (0.3–0.5 mM) was spread onto the water subphase by a microsyringe. The solvent was allowed to evaporate for at least 15 min prior to compression, and then the molecules spread on the surface were compressed at a rate of 0.1 cm 2 s $^{-1}$. The Langmuir layer was transferred onto a gold substrate (for IR reflection absorption spectroscopy (RAS) and

ellipsometry) or a slab optical waveguide of fused quartz (for UV-Vis absorption spectroscopy) by the vertical dipping method at a rate of 0.005 mm s^{-1} to prepare the LB layers. The surface pressures at transfer were 10 or 20 mN m^{-1} for **OPEn9** (LB10, LB20) and 5 mN m^{-1} for **OPEnAc**.

Preparation of SAM

A gold substrate was prepared by vapor deposition of chromium and then gold (300 and 2000 \AA for IRRAS and ellipsometry measurement, and 10 and 80 \AA for UV-Vis absorption measurement, respectively) onto a slide glass by an Osaka Vacuum N-KS350 metal deposition system. The SAM was prepared by incubating the gold substrate in a chloroform solution of **OPEn9** (0.1 mM) for 24 h . After incubation, the substrate was rinsed thoroughly with chloroform to remove physisorbed molecules and dried under a stream of nitrogen gas and in vacuum.

Characterization and spectroscopy of the layers

IRRAS of the layers on gold was performed on a Thermo Fisher Scientific Nicolet 6700 Fourier transform infrared spectrometer with a Harrick RMA-1DG/VRA reflection attachment. The incident angle was set at 85° for the LB layers and 80° for the SAM, respectively, from the surface normal. The number of interferogram accumulations was more than 200 . The tilt angles of the helix axis from the surface normal were determined from the amide I/II absorbance ratio by using an equation in the literature.²¹

The thicknesses of the layers on gold were determined by a MIZOJIRI DHA-OLX/S autoellipsometer with a helium–neon laser (632.8 nm) at an incident angle of 65° . The complex optical constant of the monolayer was assumed to be $1.50 + 0.00i$. The thickness of the monolayer was calculated automatically by an equipped program. The thicknesses were measured on 5 different spots on the surface and the data were averaged. The typical standard deviation was *ca.* 1 \AA .

The UV-Vis absorption spectrum of the **OPEn9** SAM prepared on gold was recorded on a Shimadzu UV-2450PC spectrometer with a substrate sample holder attachment at the normal incidence. The absorption spectra of the LB layers prepared on a slab optical waveguide were recorded by a System Instruments SIS-50 surface and interface spectrometer. The incident angle of the probe light was set at $17\text{--}18^\circ$ from the surface, and the accumulation number of data was 10 . The tilt angles of the long axis of the OPE from the surface normal were determined by the measurements with *p* and *s* polarizers inserted between the incident light and the sample. The tilt angles were determined from the absorbances for *p* and *s* polarized lights using an equation from the literature.²²

Results and discussion

Spectroscopy in solution

To investigate the conformation of the peptide of **OPEn9**, CD spectrum was measured in trifluoroethanol (Fig. 2). The spectrum shows a sharp negative Cotton effect at 203 nm and a broad shoulder at 224 nm . This CD pattern indicates that the peptide of **OPEn9** takes right-handed 3_{10} -helical

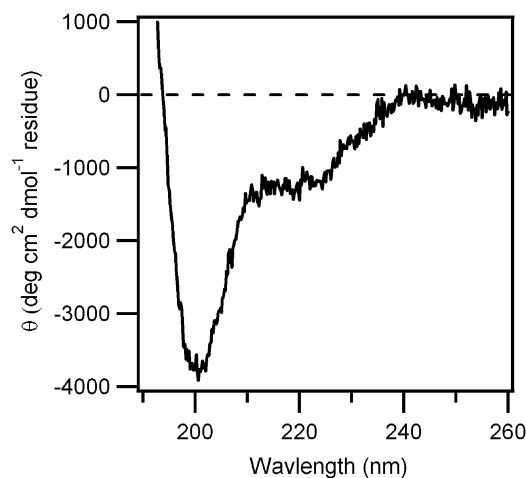


Fig. 2 CD spectrum of **OPEn9** in trifluoroethanol.

conformation²³ despite the bulky OPE component at the side chain. It is well-known that a Ala-Aib repetitive sequence favors 3_{10} -helical conformation in aprotic and less polar

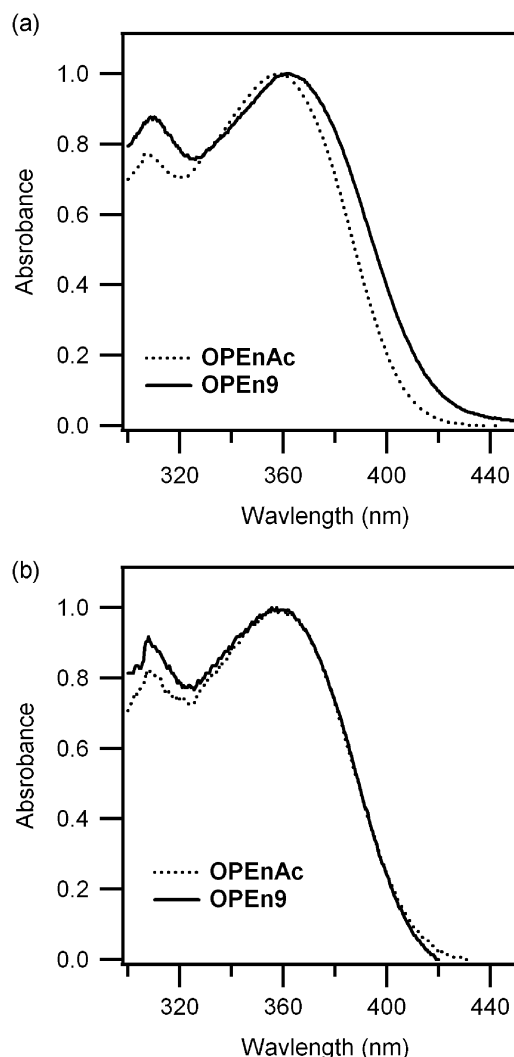


Fig. 3 UV-Vis absorption spectra of **OPEn9** and **OPEnAc** in (a) chloroform and (b) DMF.

solvents.²⁴ It is thus reasonable to consider that the peptide moiety of **OPEn9** also takes 3_{10} -helical conformation in THF and chloroform, which are aprotic and less polar than protic trifluoroethanol, and also in the layers, because they were prepared from a chloroform solution of **OPEn9**.

UV-Vis absorption spectra of **OPEn9** and **OPEnAc** in chloroform are shown in Fig. 3a. Both spectra have a broad peak with no vibration structure, which is a typical feature of OPE having a strong electron acceptor such as a nitro group.²⁵ **OPEn9** shows the maximum absorption wavelength (λ_{max}) at 364 nm, which corresponds to a red-shift of 4 nm from that of **OPEnAc** at 360 nm. This red-shift was not observed in DMF (Fig. 3b), where the dipole effect of the peptide component should be weakened due to the high dielectric constant of the medium and presumably deformation of the helical structure by DMF, which acts as hydrogen-bond donor as well as acceptor. It is considered that an electric field generated by the helical peptide dipole (Fig. 1 top) influences the electronic structure of the OPE to induce the red-shift. To validate this interpretation, *ab initio* calculations were performed.

ab initio Calculations

The geometry of **OPEnAc** was energetically optimized, and the electronic structure was determined under various electric fields by the DFT method on the B3LYP/6-31G(d,p) level. The spatial distributions of the HOMO and LUMO under no electric field and $1 \times 10^9 \text{ V m}^{-1}$ are, respectively, shown in Fig. 4. In the absence of electric field (Fig. 4 top), the HOMO is localized on the left side of the molecule and the LUMO on the other side having a nitro group. When an electric field is applied (Fig. 4 bottom), this localization of the frontier orbitals is further enhanced; the contributions of the carbon atomic orbitals on the right phenyl ring to the HOMO are reduced, whereas the contributions of the carbons on the other phenyl rings are increased. The opposite behavior is observed

for the LUMO, that is, the LUMO is further localized towards the left side carrying the nitro group. This orbital localization is also confirmed by a significant change in the magnitude of the dipole. The dipole increases from 3.75 D in the absence of electric field to 8.52 D upon applying an electric field of $1 \times 10^9 \text{ V m}^{-1}$. These results suggest that the electronic structure of the OPE component is sensitively responsive to an external electric field applied on it.

The energies of the frontier orbitals are plotted against the strength of the electric field in Fig. 5. The energies of the HOMO and LUMO are -5.77 and -2.18 eV, respectively, in the absence of an electric field. The HOMO energy level increases linearly with increase of the electric field, while the LUMO energy linearly decreases. Accordingly, the HOMO–LUMO gap reduces upon applying the electric field (Fig. 5). This behavior agrees well with the results reported by other groups.²⁶ The magnitude of the helical peptide dipole is about 20 D. The distance between the two components in the conjugate is estimated to be 0.9 nm by a molecular modeling. With using these values, the electric field generated by the peptide dipole is calculated to be $2.5 \times 10^8 \text{ V m}^{-1}$ at the center of the OPE component in case that the two dipole components are arranged in an antiparallel orientation. According to the *ab initio* calculation (Fig. 5), the HOMO–LUMO gap decreases by 0.15 eV upon applying an electric field of $2.5 \times 10^8 \text{ V m}^{-1}$. On the other hand, the experimental HOMO–LUMO gap reduction in chloroform is found to be only 0.03 eV, which is smaller than the calculated value. This discrepancy may be explained by rotational availability around the linker between the two components. The stabilization energy by the dipole–dipole interaction in the conjugate is calculated to be 6.2 kJ mol^{-1} in vacuum and 1.3 kJ mol^{-1} in chloroform (the dielectric constant of chloroform is taken to be 4.8), which is smaller than the thermal energy of 2.5 kJ mol^{-1} at 300 K. It is thus considered that the two components are allowed to rotate around the linker over the

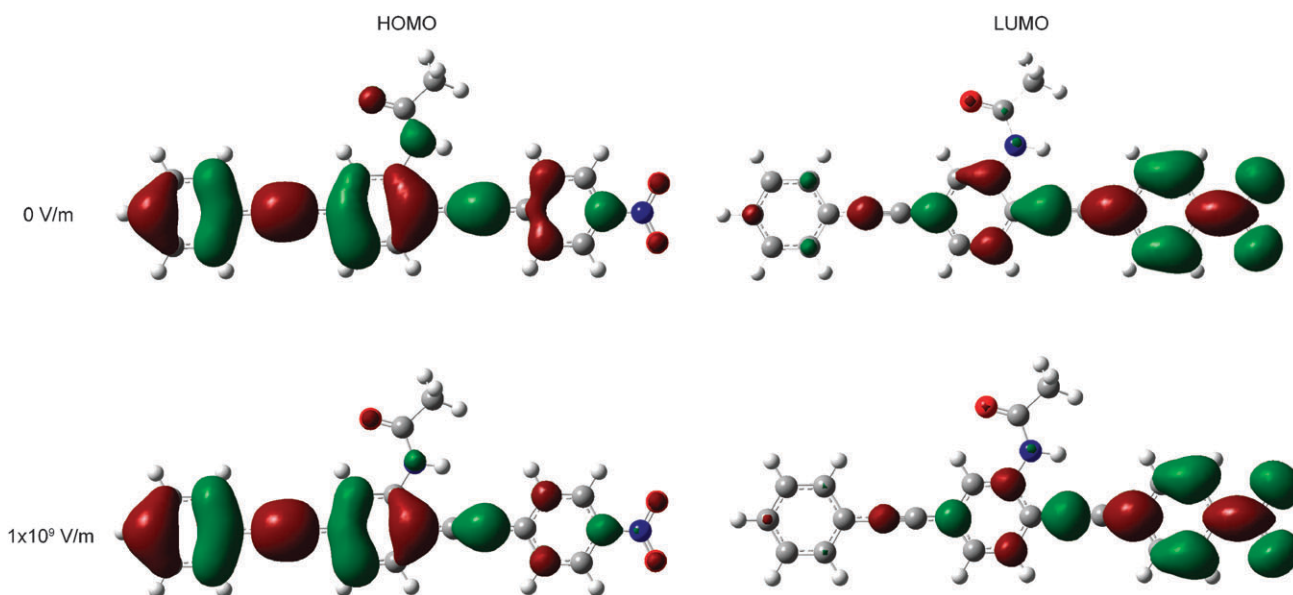


Fig. 4 Spatial distributions of the HOMO (left) and LUMO (right) of **OPEnAc** in the absence of electric field (top) and under applying an electric field of $1 \times 10^9 \text{ V m}^{-1}$ (bottom).

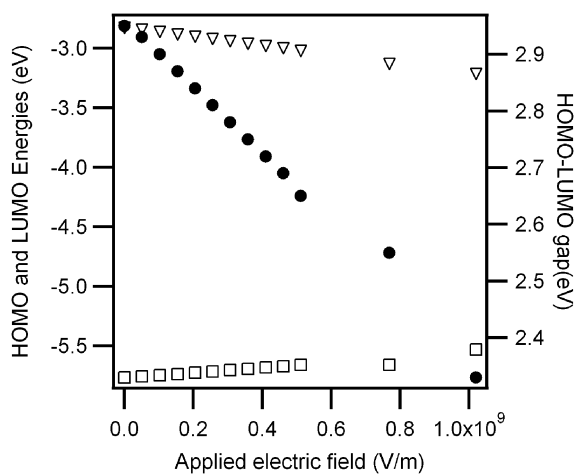


Fig. 5 Calculated energies of the HOMO (open triangle, left axis) and LUMO (open square, left axis) and HOMO–LUMO gap (filled circle, right axis) of **OPEnAc**.

small energy barrier in chloroform. It is therefore reasonable that the observed difference of the HOMO–LUMO gaps between **OPEn9** and **OPEnAc** becomes smaller than the calculated value, because all the molecules do not necessarily take the antiparallel conformation at a certain moment. Nevertheless, to our best knowledge, this is the first experimental observation of the electric field effect on the OPE electronic structure.

π -*A* Isotherm analysis

Fig. 6a shows the π -*A* isotherm of **OPEn9** at the air/water interface. Interestingly, the isotherm shows a phase transition around a molecular area of 2.2–1.3 nm² molecule⁻¹ and a surface pressure of 16 mN m⁻¹. The phase transition occurs reversibly either in the compression or the expansion process. We consider that this phase transition is due to the bilayer formation of the horizontally oriented conjugate on the subphase (Fig. 7b) as described in the next section. On the other hand, as shown in Fig. 6, each model compound for the components of **OPEn9**, **OPEnAc** and **BA8M** (Boc-(Ala-Aib)₄-OMe), does not show such a phase transition. The hysteresis observed in the isotherm of **OPEnAc** may be due to the strong stacking tendency of the OPE by π - π interaction.²⁷ The peptide component of **OPEn9** thus functions to avoid π - π stacking of the OPE upon compression on water. Furthermore, the bilayer of the conjugate does not show corruption upon compression of molecular area down to 1 nm² molecule⁻¹ with raising the surface pressure up to 20 mN m⁻¹, which makes a vivid contrast with a mixture of **OPEnAc** and **BA8M** (1/1 mol/mol) showing a very low surface pressure of 5 mN m⁻¹ upon compression to the corresponding surface area. The conjugate thus forms a stable layer, suggesting that the conjugate takes a regular structure.

Characterization of the layers

The Langmuir layer was transferred on gold or fused quartz surfaces (slab optical waveguide) by the vertical dipping method to prepare the LB layers. The surface pressures at transfers of the **OPEn9** monolayer were set at 10 or

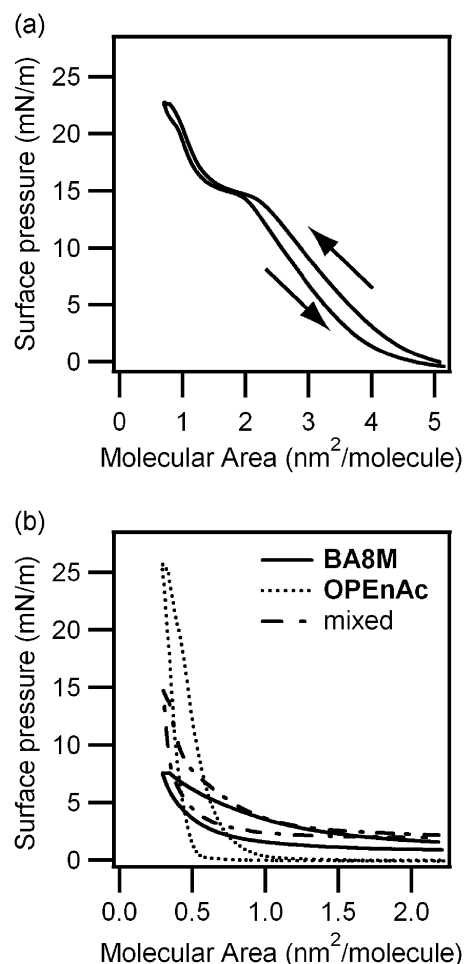


Fig. 6 π -*A* Isotherms of **OPEn9** (a), and **OPEnAc**, **BA8M**, and their mixture (b) at the air/water interface.

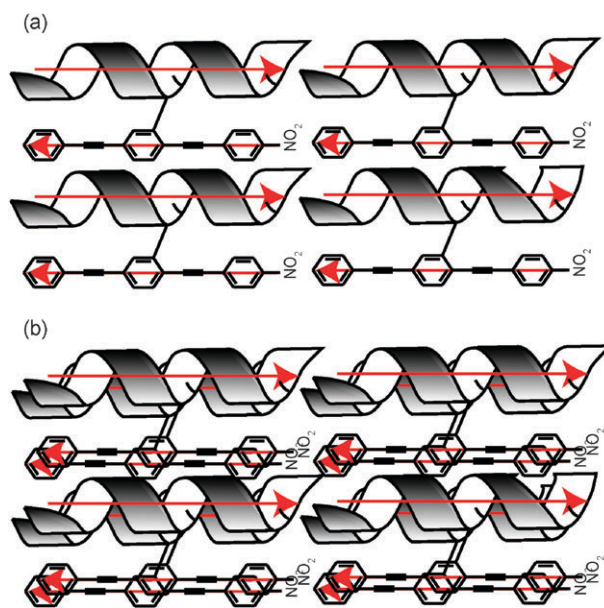


Fig. 7 Schematic representations of the top view of proposed molecular alignments of the (a) monolayer (LB10) and (b) bilayer (LB20) of **OPEn9** on an aqueous subphase or on a solid surface.

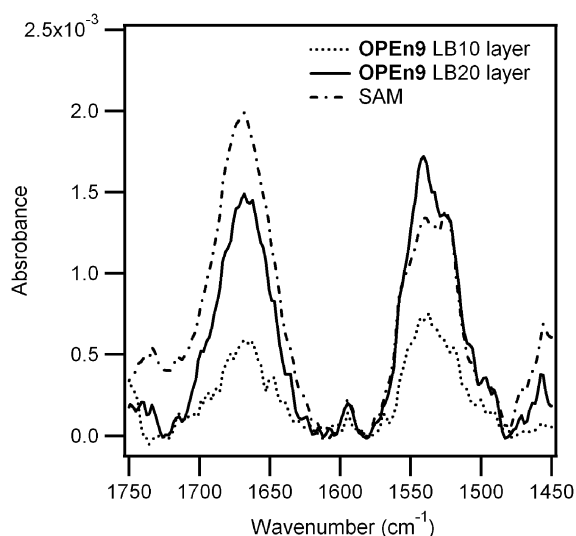


Fig. 8 IRRAS spectra of the **OPEN9** LB10 and LB20 layers, and SAM on a gold surface.

20 mN m⁻¹ (LB10, LB20). The transfer ratios of the films were near unity (1.0–1.1). On the other hand, the **OPEN9** SAM was prepared by immersion of a gold substrate into a chloroform solution of **OPEN9**. IRRAS measurements were carried out to study the molecular orientation of the peptide moiety in the **OPEN9** LB layers (LB10 and LB20) and the **OPEN9** SAM prepared on gold. The spectra are shown in Fig. 8. The amides I and II are observed at ca. 1670 and 1540 cm⁻¹, respectively. The tilt angles of the helix axis from the surface normal are determined from the amide I and II absorbance ratios to be 73° for the LB10, 69° for the LB20, and 56° for the SAM, respectively (Table 1). These results indicate that the peptide has a horizontal orientation to the surface in the LB layers even upon compression, while random orientation in the SAM. Structural irregularity of the SAM may be explained by the mismatch of the component lengths between the helical peptide and the OPE. The helical peptide is too short for the OPE to take a vertical orientation on gold.

The layer thicknesses were determined by ellipsometry to be 9 Å for LB10 and 23 Å for LB20, respectively. These values are consistent with the interpretation of monolayer and bilayer formation of the conjugate with taking horizontal orientation, when we consider the following points; (i) the diameter of a ₃₁₀ helical peptide with the repeating Ala-Aib sequence is 9.4 Å.^{6b} (ii) the OPE component should show a thinner thickness than

Table 1 λ_{max} (nm), thickness (Å), and tilt angles of the helical peptide and the OPE in various environments

	Thickness/Å	Peptide tilt angle/°	OPE tilt angle/°	λ _{max} /nm
OPENAc in chloroform	—	—	—	360
OPENAc LB	—	—	75 ± 2.0	382 ± 1.9
OPEN9 in chloroform	—	—	—	364
OPEN9 LB10	9 ± 0.5	73	74 ± 5.4	347 ± 4.6
OPEN9 LB20	23 ± 0.6	69	74 ± 3.5	358 ± 5.7
OPEN9 SAM	24 ± 0.8	56	—	335

the peptide component, (iii) both components are tilted slightly from the surface.

UV-Vis absorption spectroscopy of layers

To study the electronic structure of the OPE in the layers, the UV-vis absorption spectra were measured. The spectra are summarized in Fig. 9. The **OPEN9** SAM shows absorption maxima at 335 nm. A red-shift of 10 nm in the LB10 layer (λ_{max} = 347 nm) and a further shift of 10 nm in the LB20 layer (λ_{max} = 358 nm) are observed. As the π–A isotherm indicates that there is no π–π stacking among the OPE components in the **OPEN9** layer, we consider the red-shift as a result of the electric field effect of the peptide dipole on the OPE component in an antiparallel arrangement. To obtain information on the orientation of the OPE component, the tilt angles of the OPE long axis from the surface normal were determined by absorption anisotropy measurements using *p* and *s* linearly polarized incident lights (Table 1). The tilt angles are obtained as 73° for LB10 and 69° for LB20, respectively, indicating that the OPE component has a horizontal orientation similar to the

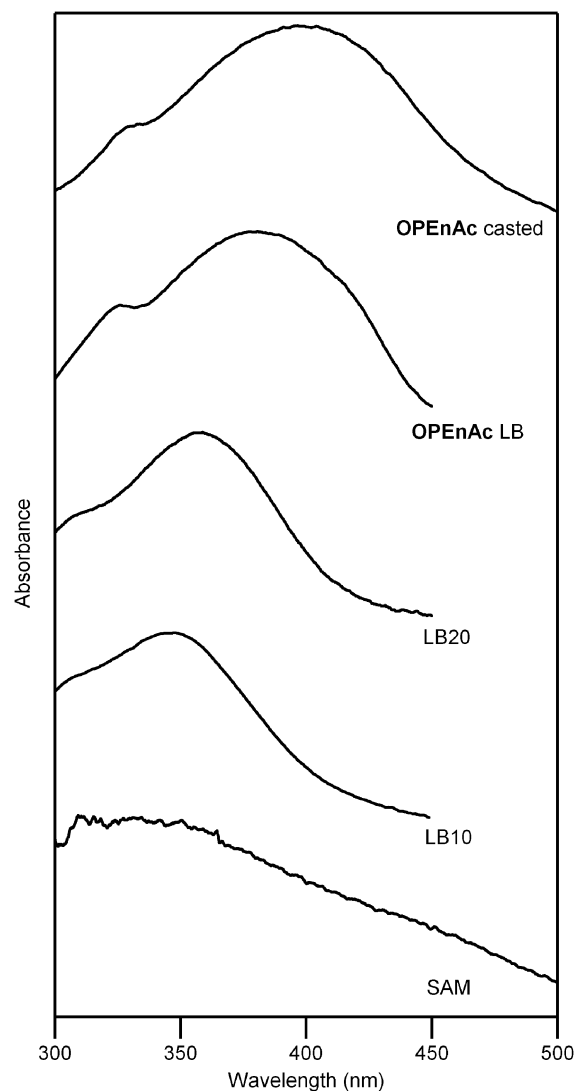


Fig. 9 UV-Vis absorption spectra of **OPENAc** and **OPEN9** in the layers.

helical peptide component. In the LB10 layer, the two components have a similar horizontal orientation to the surface. Under this geometrical constraint, the two components in the conjugate should favor antiparallel arrangement. Furthermore, head-to-tail arrangement in the layer may be prevailing because of stabilization of dipole–dipole interaction as depicted in Fig. 7a. This type of head-to-tail arrangement was previously reported in a LB monolayer of a 24mer helical peptide.²⁸ The red-shift of 10 nm is thus caused by the electric field generated by the peptide dipoles neighboring the OPE. In the LB20 layer, the conjugates are piled up to double with keeping the horizontal and the antiparallel arrangement (Fig. 7b). The electric field strength around the OPE thus becomes double to induce another red-shift of 10 nm. On the other hand, in the SAM, the peptide components orient randomly on the surface. Although the orientation of the OPE component in the SAM could not be measured, it is plausibly considered that the relative orientation of the OPE to the peptide is random because of random distribution of the surrounding dipoles.

Another possible explanation for the red-shift of the OPE component in the LB10 and LB20 layers might be due to the π – π stacking of the OPE. Indeed, in the cases of the **OPENAc** LB layer and cast film, large red-shifts of 47 and 59 nm, respectively, from the λ_{max} in the **OPEN9** SAM were observed (Fig. 9). The electronic structure of OPE changes with variation of the dihedral angle between neighboring phenyl planes.²⁹ The HOMO–LUMO gap of OPE is the smallest when the molecule takes a coplanar geometry, while it becomes the largest with orthogonal orientation of the neighboring phenyl planes. The rotation of the phenyl rings around the ethynylene axis is known to be nearly frictionless in a dilute solution.^{27a,29c,30} In the LB layer of **OPENAc**, however, the molecules tend to stack with each other to induce a red-shift in the absorption spectrum by taking a coplanar geometry. Hu *et al.* clarified this relation of λ_{max} with the coplanarity recently.³¹ However, this reason is considered to be excluded from the explanation of the red shift in the **OPEN9** layers, because π – π stacking of the conjugate in those layers is not significant as revealed by the reversible π – A isotherms, which is described in the previous section.

Conclusion

A novel conjugate of OPE and a helical peptide was synthesized and studied on the dipole effect of the helical peptide on the electronic structure of the OPE and a dipole–dipole interaction in regulation of the molecular structure. In chloroform, the conjugate showed a red-shifted absorption compared to a reference OPE derivative, indicating that the electric field effect of the helical peptide dipole on the electronic structure of the OPE in the conjugate appeared, where both components favored an antiparallel arrangement due to the dipole–dipole interaction. This interpretation was supported by *ab initio* calculations. In the LB layers of the conjugate, the red-shifts of the λ_{max} became larger than that in chloroform because of the additive dipole effects from the helical peptides neighboring the OPE. We are now working on clarification of the precise molecular alignment in the LB

layers using scanning probe microscopies of STM and AFM. Another novel conjugate is under investigation, where the two components are connected at two sites to fix the antiparallel arrangement. The dipole effect on the OPE will appear more prominent than in the present case.

Acknowledgements

This work is partly supported by Grant-in-Aids for Exploratory Research (17655098), and for Scientific Research B (15350068), and Global COE program, International Center for Integrated Research and Advanced Education in Materials Science, from the Ministry of Education, Culture, Sports, Science, and Technology, Japan.

References

- (a) V. Torchilin, *Pharm. Res.*, 2007, **24**, 1–16; (b) M. Staples, K. Daniel, M. Cima and R. Langer, *Pharm. Res.*, 2006, **23**, 847–863.
- (a) E. Gomar-Nadal, J. Puigmarti-Luis and D. B. Amabilino, *Chem. Soc. Rev.*, 2008, **37**, 490–504; (b) S. Roy, *J. Phys. D: Appl. Phys.*, 2007, **40**, R413; (c) ed. R. Waser, *Nanoelectronics and Information Technology*, WILEY-VCH Verlag GmbH & Co. KGaA, Weinheim, 2nd, corrected edn, 2005.
- G. Moore, *Electronics*, 1965, **38**, 114–117.
- E. M. Vogel, *Nat. Nanotechnol.*, 2007, **2**, 25–32.
- (a) F. D. Lewis, T. Wu, Y. Zhang, R. L. Letsinger, S. R. Greenfield and M. R. Wasielewski, *Science*, 1997, **277**, 673–676; (b) R. E. Holmlin, P. J. Dandliker and J. K. Barton, *Angew. Chem. Int. Ed. Engl.*, 1997, **36**, 2714–2730; (c) P. Lincoln, E. Tuite and B. Norden, *J. Am. Chem. Soc.*, 1997, **119**, 1454–1455.
- (a) T. Morita and S. Kimura, *J. Am. Chem. Soc.*, 2003, **125**, 8732–8733; (b) M. Kai, K. Takeda, T. Morita and S. Kimura, *J. Pept. Sci.*, 2008, **14**, 192–202; (c) K. Takeda, T. Morita and S. Kimura, *J. Phys. Chem. B*, 2008, **112**, 12840–12850; (d) S. Sek, A. Tolak, A. Misicka, B. Palys and R. Bilewicz, *J. Phys. Chem. B*, 2005, **109**, 18433–18438; (e) M. M. Galka and H. Kraatz, *ChemPhysChem*, 2002, **3**, 356–359.
- (a) A. Aviram and M. A. Ratner, *Chem. Phys. Lett.*, 1974, **29**, 277–283; (b) R. Metzger, B. Chen, U. Hopfner, M. Lakshminantham, D. Vuillaume, T. Kawai, X. Wu, H. Tachibana, T. Hughes, H. Sakurai, J. Baldwin, C. Hosch, M. Cava, L. Brehmer and G. Ashwell, *J. Am. Chem. Soc.*, 1997, **119**, 10455–10466; (c) R. M. Metzger, *Chem. Phys.*, 2006, **326**, 176–187.
- (a) R. A. Bissell, E. Cordova, A. E. Kaifer and J. F. Stoddart, *Nature*, 1994, **369**, 133–137; (b) J. E. Green, J. Wook Choi, A. Boukai, Y. Bunimovich, E. Johnston-Halperin, E. DeIonno, Y. Luo, B. A. Sheriff, K. Xu, Y. Shik Shin, H. Tseng, J. F. Stoddart and J. R. Heath, *Nature*, 2007, **445**, 414–417; (c) W. R. Dichtel, J. R. Heath and J. Fraser Stoddart, *Phil. Trans. R. Soc. A*, 2007, **365**, 1607–1625; (d) I. Poleschak, J. Kern and J. Sauvage, *Chem. Commun.*, 2004, 474–476.
- (a) E. Kay, D. Leigh and F. Zerbetto, *Angew. Chem., Int. Ed.*, 2007, **46**, 72–191; (b) C. P. Collier, G. Mattersteig, E. W. Wong, Y. Luo, K. Beverly, J. Sampaio, F. M. Raymo, J. F. Stoddart and J. R. Heath, *Science*, 2000, **289**, 1172–1175; (c) D. Payer, S. Rauschenbach, N. Malinowski, M. Konuma, C. Virojanadara, U. Starke, C. Dietrich-Buchecker, J. Collin, J. Sauvage, N. Lin and K. Kern, *J. Am. Chem. Soc.*, 2007, **129**, 15662–15667.
- (a) W. B. Davis, W. A. Svec, M. A. Ratner and M. R. Wasielewski, *Nature*, 1998, **396**, 60–63; (b) H. D. Sikes, J. F. Smalley, S. P. Dudek, A. R. Cook, M. D. Newton, C. E. D. Chidsey and S. W. Feldberg, *Science*, 2001, **291**, 1519–1523; (c) P. Hedegård and T. Bjørnholm, *Chem. Phys.*, 2005, **319**, 350–359; (d) M. D. Newton and J. F. Smalley, *Phys. Chem. Chem. Phys.*, 2007, **9**, 555–572; (e) A. Danilov, S. Kubatkin, S. Kafanov, P. Hedegård, N. Stühr-Hansen, K. Moth-Poulsen and T. Bjørnholm, *Nano Lett.*, 2008, **8**, 1–5.

- 11 (a) L. A. Bumm, J. J. Arnold, M. T. Cygan, T. D. Dunbar, T. P. Burgin, L. Jones II, D. L. Allara, J. M. Tour and P. S. Weiss, *Science*, 1996, **271**, 1705–1707; (b) J. M. Tour, A. M. Rawlett, M. Kozaki, Y. Yao, R. C. Jagessar, S. M. Dirk, D. W. Price, M. A. Reed, C.-W. Zhou, J. Chen, W. Wang and I. Campbell, *Chem.–Eur. J.*, 2001, **7**, 5118–5134; (c) C. D. Zangmeister, S. W. Robey, R. D. van Zee, Y. Yao and J. M. Tour, *J. Phys. Chem. B*, 2004, **108**, 16187–16197; (d) S. B. Sachs, S. P. Dudek, R. P. Hsung, L. R. Sita, J. F. Smalley, M. D. Newton, S. W. Feldberg and C. E. D. Chidsey, *J. Am. Chem. Soc.*, 1997, **119**, 10563–10564; (e) Y. Selzer, L. Cai, M. A. Cabassi, Y. Yao, J. M. Tour, T. S. Mayer and D. L. Allara, *Nano. Lett.*, 2005, **5**, 61–65; (f) A. M. Moore, B. A. Mantooth, Z. J. Donhauser, Y. Yao, J. M. Tour and P. S. Weiss, *J. Am. Chem. Soc.*, 2007, **129**, 10352–10353.
- 12 (a) J. Zhu, X. Wang, Y. Chen, X. Jiang, X. Chen and Z. Li, *J. Org. Chem.*, 2004, **69**, 6221–6227; (b) W. Hu, N. Zhu, W. Tang and D. Zhao, *Org. Lett.*, 2008, **10**, 2669.
- 13 M. Cubberley and B. Iverson, *J. Am. Chem. Soc.*, 2001, **123**, 7560–7563.
- 14 D. J. Hill and J. S. Moore, *Proc. Natl. Acad. Sci. U. S. A.*, 2002, **99**, 5053–5057.
- 15 T. Ishikawa, T. Morita and S. Kimura, *Bull. Chem. Soc. Jpn.*, 2007, **80**, 1483–1491.
- 16 S. Kimura, *Org. Biomol. Chem.*, 2008, **6**, 1143–1148.
- 17 M. J. Frisch, G. W. Trucks, H. B. Schlegel, G. E. Scuseria, M. A. Robb, J. R. Cheeseman, J. A. Montgomery, Jr, T. Vreven, K. N. Kudin, J. C. Burant, J. M. Millam, S. S. Iyengar, J. Tomasi, V. Barone, B. Mennucci, M. Cossi, G. Scalmani, N. Rega, G. A. Petersson, H. Nakatsuji, M. Hada, M. Ehara, K. Toyota, R. Fukuda, J. Hasegawa, M. Ishida, T. Nakajima, Y. Honda, O. Kitao, H. Nakai, M. Klene, X. Li, J. E. Knox, H. P. Hratchian, J. B. Cross, V. Bakken, C. Adamo, J. Jaramillo, R. Gomperts, R. E. Stratmann, O. Yazyev, A. J. Austin, R. Cammi, C. Pomelli, J. W. Ochterski, P. Y. Ayala, K. Morokuma, G. A. Voth, P. Salvador, J. J. Dannenberg, V. G. Zakrzewski, S. Dapprich, A. D. Daniels, M. C. Strain, O. Farkas, D. K. Malick, A. D. Rabuck, K. Raghavachari, J. B. Foresman, J. V. Ortiz, Q. Cui, A. G. Baboul, S. Clifford, J. Cioslowski, B. B. Stefanov, G. Liu, A. Liashenko, P. Piskorz, I. Komaromi, R. L. Martin, D. J. Fox, T. Keith, M. A. Al-Laham, C. Y. Peng, A. Nanayakkara, M. Challacombe, P. M. W. Gill, B. Johnson, W. Chen, M. W. Wong, C. Gonzalez and J. A. Pople, *GAUSSIAN 03 (Revision E.01)*, Gaussian Inc., Wallingford, CT, 2004.
- 18 A. D. Becke, *J. Chem. Phys.*, 1993, **98**, 5648–5652.
- 19 R. Ditchfield, W. J. Hehre and J. A. Pople, *J. Chem. Phys.*, 1971, **54**, 724–728.
- 20 R. Dennington II, T. Keith and J. Millam, *GaussView Version 4.1*, Semichem, Inc., Shawnee Mission, KS, 2007.
- 21 (a) H. U. Gremlich, U. P. Fringeli and R. Schwyter, *Biochemistry*, 1983, **22**, 4257–4264; (b) Y. Miura, S. Kimura, Y. Imanishi and J. Umemura, *Langmuir*, 1998, **14**, 6935–6940.
- 22 F. Li and R. Zare, *J. Phys. Chem. B*, 2005, **109**, 3330–3333.
- 23 C. Toniolo, A. Polese, F. Formaggio, M. Crisma and J. Kamphuis, *J. Am. Chem. Soc.*, 1996, **118**, 2744–2745.
- 24 D. F. Kennedy, M. Crisma, C. Toniolo and D. Chapman, *Biochemistry*, 1991, **30**, 6451–6548.
- 25 (a) H. Meier, B. Mühling and H. Kolshorn, *Eur. J. Org. Chem.*, 2004, 1033–1042; (b) C. Risko, C. D. Zangmeister, Y. Yao, T. J. Marks, J. M. Tour, M. A. Ratner and R. D. van Zee, *J. Phys. Chem. C*, 2008, **112**, 13215–13225.
- 26 (a) X. Yin, Y. Li, Y. Zhang, P. Li and J. Zhao, *Chem. Phys. Lett.*, 2006, **422**, 111–116; (b) Y. Li, J. Zhao, X. Yin and G. Yin, *J. Phys. Chem. A*, 2006, **110**, 11130–11135; (c) A. Staykov, D. Nozaki and K. Yoshizawa, *J. Phys. Chem. C*, 2007, **111**, 11699–11705.
- 27 (a) T. Miteva, L. Palmer, L. Kloppenburg, D. Neher and U. H. F. Bunz, *Macromolecules*, 2000, **33**, 652–654; (b) C. Halkyard, M. Rampey, L. Kloppenburg, S. Studer-Martinez and U. Bunz, *Macromolecules*, 1998, **31**, 8655–8659; (c) S. Masuo, H. Yoshikawa, T. Asahi, H. Masuhara, T. Sato, D. Jiang and T. Aida, *J. Phys. Chem. B*, 2003, **107**, 2471–2479.
- 28 N. Morino, K. Kitagawa, T. Morita and S. Kimura, *Thin Solid Films*, 2005, **479**, 261–268.
- 29 (a) M. I. Sluch, A. Gold, U. H. F. Bunz and M. A. Berg, *J. Am. Chem. Soc.*, 2001, **123**, 6447–6448; (b) E. Nesterov, Z. Zhu and T. Swager, *J. Am. Chem. Soc.*, 2005, **127**, 10083–10088; (c) J.-S. Yang, J.-L. Yan, C.-Y. Hwang, S.-Y. Chiou, K.-L. Liao, H.-H. G. Tsai, G.-H. Lee and S.-M. Peng, *J. Am. Chem. Soc.*, 1996, **118**, 14109–14119.
- 30 (a) A. Satrijo and T. M. Swager, *J. Am. Chem. Soc.*, 2007, **129**, 16020–16028; (b) K. Kim and T. M. Swager, *Nature*, 2001, **411**, 1030–1034.
- 31 W. Hu, N. Zhu, W. Tang and D. Zhao, *Org. Lett.*, 2008, **10**, 2669–2672.